

## Optical nanospectroscopy study of ion-implanted silicon and biological growth medium

A. Cricenti<sup>a,\*</sup>, V. Marocchi<sup>a</sup>, R. Generosi<sup>a</sup>, M. Luce<sup>a</sup>, P. Perfetti<sup>a</sup>, D. Vobornik<sup>b</sup>,  
G. Margaritondo<sup>b</sup>, D. Talley<sup>c</sup>, P. Thielen<sup>c</sup>, J.S. Sanghera<sup>c</sup>,  
I.D. Aggarwal<sup>c</sup>, J.K. Miller<sup>d</sup>, N.H. Tolk<sup>d</sup>, D.W. Piston<sup>e</sup>

<sup>a</sup> *Istituto di Struttura della Materia, via Fosso del Cavaliere 100, 00133 Rome, Italy*

<sup>b</sup> *Institut de physique appliquée, Ecole Polytechnique Fédérale, CH-1015 Lausanne, Switzerland*

<sup>c</sup> *Optical Sciences Division, U.S. Naval Research Laboratory, 4555 Overlook Ave SE, Washington, DC 20375, USA*

<sup>d</sup> *Department of Physics and Astronomy, Vanderbilt University, Nashville, TN 31235, USA*

<sup>e</sup> *Department of Molecular Physiology and Biophysics, Vanderbilt University, Nashville, TN 37232, USA*

Received 10 September 2002; received in revised form 15 January 2003; accepted 20 January 2003

### Abstract

The advent of scanning near-field optical microscopy (SNOM) has augmented at the microscopic level the usefulness of IR spectroscopy. Two-dimensional imaging of chemical constituents makes this a very attractive and powerful new approach. In this paper we present SNOM results on boron-doped silicon and on biological growth medium by means of shear-force, reflectivity and photocurrent measurements. Such experiments allowed us to identify boron clusters embedded in silicon and the distribution of growth medium constituents with a lateral resolution well below the diffraction limit.

© 2003 Elsevier B.V. All rights reserved.

*Keywords:* Nanostructures; Scanning near-field optical microscopy; Internal photoemission; Reflectivity

### 1. Introduction

Optical spectroscopy is an excellent probe of semiconductor interfaces, whose energy barriers and discontinuities fall in its spectral domain [1,2]. Contrary to conventional electron spectroscopy approaches, the optical radiation has a deep penetration and can analyze technologically realistic buried interfaces [2]. These investigations, however, are affected by a severe limitation common to many other interface studies: lack of lateral resolution. In fact, classical optical microscopy finds its limit in the inability of separating two objects located at distance smaller than half the wavelength  $\lambda$  of the light involved. The Rayleigh criterion establishes that two points are distinguishable only if the distance between them is larger than  $\lambda/(2n \sin \theta)$  where  $n$  is the refractive index of the medium and  $\theta$  is half the aperture angle of the optical system. In real systems, many in-

terface properties and phenomena change significantly from place to place [3,4]. So that, the lack of lateral resolution may lead to misleading or incomplete results, and makes it impossible to really understand many microelectronics devices. The infrared (IR) absorption of a biological system can potentially probe fine and fundamentally important microchemical properties, for example, by monitoring intracellular metabolism and signal transmission. However, the practical implementation of this approach has been so far problematic because of the need for high lateral resolution and because of the diffraction limit of conventional infrared microscopy.

This limitation can be removed by using a SNOM apparatus where a stretched optical fiber with a very small open edge aperture collects the reflected radiation—thereby reaching resolution levels beyond the diffraction limit [5]. In fact, the SNOM technique is growing rapidly in importance for characterizing materials with spatial resolution far below the classical diffraction limit [5–7]. This technique offers a unique opportunity for nondestructively studying localized variations in buried interfaces [8] and biological samples.

\* Corresponding author. Fax: +39-064-993-4153.

E-mail address: cricenti@nameserver.ism.rm.cnr.it (A. Cricenti).

In this paper we show results on boron-doped silicon and on biological growth medium by means of shear-force, reflectivity and photocurrent measurements. In both cases, we observed photocurrent and/or reflectivity features which do not match topographic structures in the shear-force images. Such experiments allowed us to identify boron clusters embedded in silicon and the distribution of growth medium constituents with a lateral resolution well below the diffraction limit.

## 2. Experimental set-up

The SNOM unit has been described in Ref. [9] and is made of two separate parts: a lower part and an upper one. The fibre tip fits tightly into a small tube mechanically attached to a stainless steel piece rigidly connected to the top part. The two parts are held together by a pivot on one side, and by a screw lock on the other used for a rough approach between tip and sample and to ensure a rigid connection between the two halves so resulting in a low noise apparatus. The two parts contain the sample holder, a piezoelectric scanner, and  $x$ - $y$ - $z$  motor-controlled translators. The sample holder permits to accommodate specimens several centimetres large. The piezo-scanner allows the  $x$ ,  $y$ ,  $z$  motions with an available  $z$ -motion of  $\sim 5 \mu\text{m}$  whereas the  $x$ ,  $y$  scanning motion is  $\sim 34 \mu\text{m}$  for each axis. The piezo-scanner is fixed onto an  $x$ ,  $y$ ,  $z$  translator and can be moved  $\pm 4 \text{ mm}$  along the  $x$ ,  $y$  direction by two continuous motors and  $\pm 1 \text{ mm}$  along the  $z$  direction.

The variation of tip-sample distance during  $x$ ,  $y$  motion is compensated by moving the  $z$  motor. A feedback circuit operates in such a way that as the sample approaches the fibre and a change in the shear-force amplitude is detected, the feedback circuit becomes active and the stepping is halted. This method is able to avoid fibre crashing onto the specimen.

The instrument allows to measure the reflectivity of the sample with the optical fibre when the surface is illumi-

nated by an external source or by light coming from the optical fibre itself. Also photocurrent measurements can be performed directly illuminating the sample by the fibre. In this case the back contact of the specimen is directly fed to an  $I$ - $V$  converter preamplifier with a fixed gain that reveal the electron current induced by the incoming photons. In Fig. 1 the schematics of the set-up are shown.

## 3. Results

### 3.1. Boron-doped silicon

A combination of internal photoemission (IPE) and SNOM has been used to investigate the electronic properties of silicon after boron implantation and annealing. Three different wavelengths have been used [633 nm (not shown), 1330 nm and 1550 nm (not shown)] to locally illuminate the sample. Shear-force (SF), reflectivity (R) and photocurrent (PC) images were collected simultaneously and compared in order to discriminate between true structures and artifacts. For the acquisition of R images the tapered optical fiber locally illuminates the sample and collects the light normally reflected at the surface by means of a fiber coupler. The topography image was acquired by monitoring the tip position with a shear-force control system and the photocurrent signal was measured by an  $I/V$  converter preamplifier with a fixed gain ( $10^8 \text{ V/A}$ ).

$\text{B}^+$  ion implantation in silicon is the most useful p-type doping process and it is crucial to determine as-implanted and postanneal impurity distributions with the highest possible accuracy. Since implantation of energetic ions into silicon induces a large amount of crystal damage in the semiconductor consisting of high concentrations of interstitials and vacancies much higher than the implant dose, rapid thermal annealing is used to restore lattice order and to achieve dopant activation. Any annealing step is a highly nonequilibrium process and involves the formation/dissolution of extended defects, metastable phases and precipitates. As a

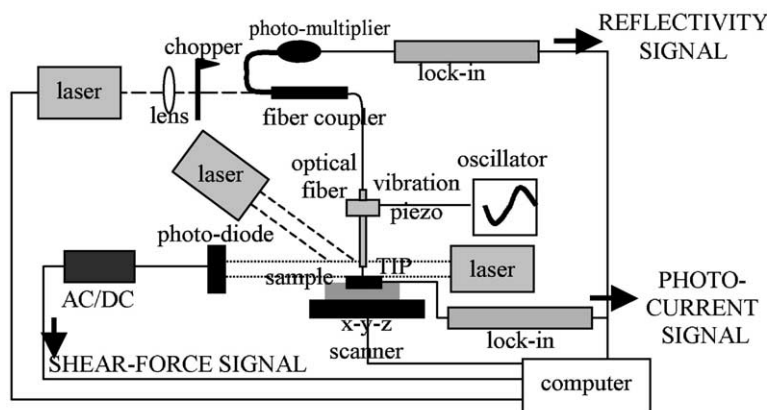


Fig. 1. Experimental set-up.

result, both point defects and dopant atoms experience a high mobility characterized by anomalous diffusion, namely transient enhanced diffusion. Dopant atoms may also form inactive immobile clusters and may deactivate much below their solid solubility. Since the solid solubility of B in Si is limited to  $2 \times 10^{20}$  atoms/cm<sup>3</sup>, for increasingly high implant doses, there is an increasing tendency for impurity atoms to cluster within the Si lattice after annealing. Depending on the level of boron concentration the photocurrent shows intensity varying between two orders of magnitude. Boron clusters behave as metal clusters embedded into the silicon matrix and introduce gap states which give rise to the observed photocurrent. The images here reported are for a Si(100) sample with the mean B-concentration values concerning the first 1  $\mu\text{m}$  of depth of  $\sim 5 \cdot 10^{19}$  cm<sup>-3</sup>.

Fig. 2 shows a  $10 \times 10 \mu\text{m}$  image of the shear-force (a), reflectivity (b) and photocurrent (c) taken with a photon wavelength of 1330 nm, that is below the indirect band gap of silicon: as visible, there is no correspondence between the SF and PC images acquired on the same silicon sample scanned area. As evidenced by the white traces (AA') outlined in

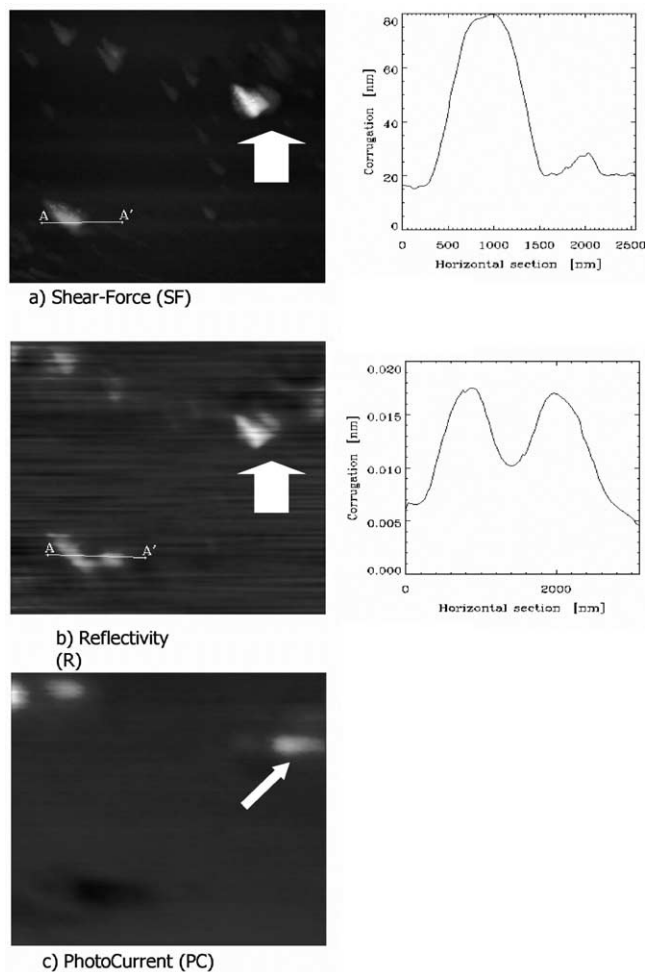


Fig. 2. Shear-force (a), Reflectivity (b), PhotoCurrent (c) images acquired on the same silicon sample area with a photon of  $\lambda = 1330$  nm.

both the images, there is a reflectivity enhancement with no correspondence in the SF image and that might be due to a subsurface defect. The SF and R images show surface related structures not related to B and give rise to local minima in the PC image due, probably, to scattering of the impinging light. The PC image shows the presence of a buried B cluster which has no correspondence in the SF and R images and is characterized by lateral dimensions of several hundred nanometers. It has to be mentioned that they are certainly affected by the convolution of the tip aperture with the penetration depth  $\alpha = \lambda/4\pi k$  of the light and by the subsequent diffusion of the excited carriers from the excitation volume. A resolution less than 100 nm (that is  $\sim \lambda/13$ ) is observable in both the R and the PC images that have been collected in many different areas of the sample.

### 3.2. Biological material

An important first step in the evaluation of biological structures is the IR characterization of the biological growth medium. The growth medium is composed of several products [10], primarily sulphur and nitrogen oxide compounds, whose vibrational stretch mode absorption bands occur in the infrared around 7  $\mu\text{m}$  [11]. SNOM images were taken by tuning the Free electron laser (FEL) to  $\lambda = 6.95 \mu\text{m}$ , i.e. at such absorption band, and at 6.6  $\mu\text{m}$ , i.e. outside the absorption band, in order to estimate the noise-background contributions. A major requirement is a suitable IR photon source: which is both intense and tunable. Tunability is required to cover the relevant absorption bands. Intensity is a critical point because of the inefficient light transmission of the narrow fiber tip. FEL sources are ideal for this problem because of their unique combination of extreme intensity and broad tunability. The FEL photons are sent to the sample surface, and detected after reflection by the narrow-point optical fiber tip mounted on our SNOM module.

Fig. 3 (left-hand side) shows two  $20 \times 20 \mu\text{m}^2$  SNOM reflection images obtained with  $\lambda = 6.95 \mu\text{m}$  photons (image c) and with the adjacent wavelength,  $\lambda = 6.6 \mu\text{m}$  (image a). In the reflection images darker areas correspond to stronger absorption. The contrast between the featureless image off-absorption and the microstructures of the on-absorption image is striking. Are these microstructures really related to the growth medium constituents or are they just artifacts? To answer this question we compare the corresponding shear-force (topological) image of Fig. 3b. First of all the same topological image is observed at the two different wavelengths (image b). The topological images show the presence of several biological growth medium grains with width and height of few micrometers. Furthermore, if we are dealing with artifacts, we would expect a similar optical image when collecting data at 6.6  $\mu\text{m}$  (image c) and 6.95  $\mu\text{m}$  (image a): absolutely no one-to-one correlation is observed between the two SNOM images, ruling out artifacts. This proves, in fact, that the dark regions in the on-absorption SNOM image of Fig. 3c correspond to regions with strong

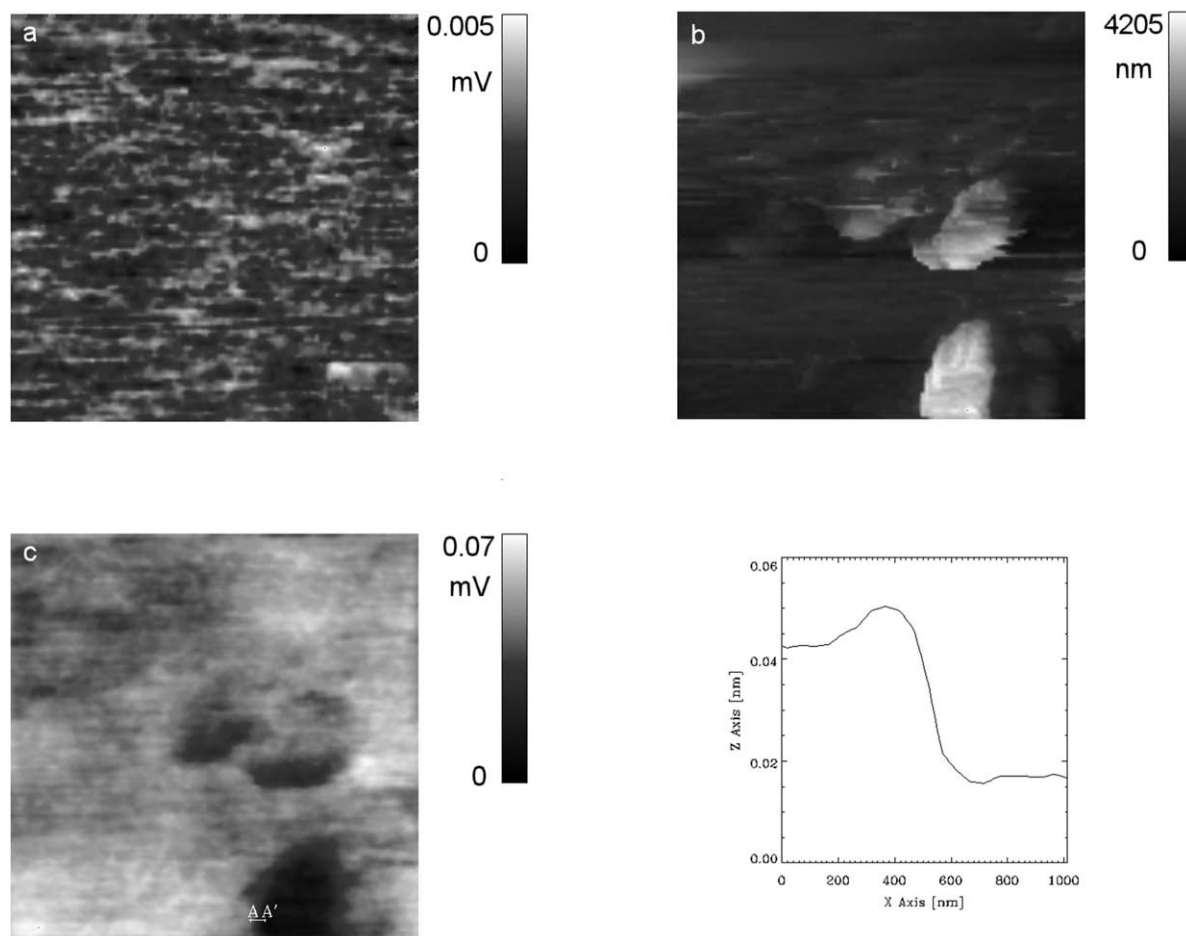


Fig. 3. Left:  $20 \times 20 \mu\text{m}^2$  SNOM reflection images obtained with  $\lambda = 6.95 \mu\text{m}$  photons (3c), corresponding to the vibrational stretch mode absorption bands of sulphur and nitrogen oxide compounds, and with an adjacent wavelength outside the absorption band,  $\lambda = 6.6 \mu\text{m}$  (3a). Darker areas correspond to stronger absorption. Right: Corresponding shear-force (topographic) image (3b); brighter areas correspond to higher topography values. All the images shown are unfiltered and raw except for subtraction of a constant background. Also shown is the profile taken along the A–A' line on the reflectivity image taken with  $\lambda = 6.95 \mu\text{m}$  in Fig. 3c.

growth medium component concentrations related absorption.

It is quite instructive to analyse the lateral resolution of the topographic and spectroscopic-SNOM images obtained in this work. For the topographic images, line scans yield a lateral resolution of between 50 and 80 nm, demonstrating the high quality of the fiber tips. On the other hand, similar line scans for the spectroscopic SNOM images (see the slope in the profile A–A') demonstrate a lateral resolution of 200 nm, which is well below the classical-microscopy limit ( $\lambda/2$ ). A lateral resolution value better than  $\lambda/30$  was obtained at  $6.95 \mu\text{m}$ .

#### 4. Summary

In conclusion, we have presented SNOM results on boron-doped silicon and on biological cells by means of shear-force, reflectivity and photocurrent measurements.

This approach allowed us to identify boron clusters embedded in silicon with a lateral resolution better than 100 nm. Moreover, the results clearly reveal different chemical constituents in a biological growth medium film: this chemical sensitivity, with a lateral resolution of  $0.2 \mu\text{m}$  ( $\approx \lambda/35$ ), is well below the diffraction limit of standard microscopy.

The potential applications of this approach touch virtually every aspect of the life sciences and medical research, as well as problems in materials science, chemistry, physics and environmental research.

#### Acknowledgements

We would like to thank the entire staff of the Vanderbilt FEL center for their able assistance. This work is supported by the Italian National Research Council (CNR), by the Ecole Polytechnique Fédérale de Lausanne and by the Fonds National Suisse de la Recherche Scientifique. The Vanderbilt

FEL center is a national facility supported by the US Office of Naval Research.

## References

- [1] E. Yuncel, et al., *Phys. Rev. Lett.* 70 (1993) 4146.
- [2] C. Coluzza, et al., *Phys. Rev. B* 46 (1992) 12834.
- [3] C. Coluzza, et al., *J. Appl. Phys.* 76 (1994) 3710.
- [4] G. Margaritondo, F. Gozzo, C. Coluzza, *Phys. Rev. B* 47 (1993) 9907.
- [5] A detailed discussion of the mechanism of optical contrast observed in SNOM images can be found in: NATO ASI Series Near Field Optics, D.W. Pohl, D. Courjon (Editors), Kluwer Academic Press (1992) Vol. 262.
- [6] E. Betzig, P.L. Finn, J.S. Wiener, *Appl. Phys. Lett.* 60 (1994) 2484.
- [7] J. Almeida, et al., *Appl. Phys. Lett.* 69 (1996) 2361.
- [8] C. Coluzza, J. Almeida, T. dell'Orto, O. Bergossi, M. Spajer, S. Davy, D. Courjon, A. Cricenti, R. Generosi, P. Perfetti, G. Faini, *SPIE* 2782 (1997) 591.
- [9] A. Cricenti, R. Generosi, C. Barchesi, M. Luce, M. Rinaldi, *Rev. Sci. Instrum.* 69 (1998) 3240.
- [10] D. de Beer, P. Stoodley, F. Roe, Z. Lewandowski, *Biotechnol. Bioeng.* 43 (1994) 1131.
- [11] H. van der Maas, *Basic Infrared Spectroscopy*, 2nd Edition, Heyden, London, 1972, pp. 88–89.